Influence of Heat Release on Swirl Flow Dynamics From High Speed Laser Measurements in a Gas Turbine Model Combustor

Christoph M. Arndt, Adam M. Steinberg, Isaac G. Boxx, Wolfgang Meier, Manfred Aigner
German Aerospace Center (DLR), Institute of Combustion Technology
Pfaffenwaldring 38-40, D-70569 Stuttgart, Germany

1 Introduction

Swirl burners are often utilized in practical combustors, such as those found in gas turbines (GT), because swirl-induced vortex breakdown presents an effective mechanism for flame anchoring and stabilization [1, 2]. Vortex breakdown is often accompanied by coherent helical structures termed precessing vortex cores (PVC), which spiral around the flame axis in the shear layer between the inflow and the inner recirculation zone [3]. While PVCs are frequently identified in non-reacting swirl flows [4–6], their appearance in swirl flames has been reported to a lesser extent [7, 8]. In several experimental and numerical investigations, it was shown that a PVC present in a non-reacting flow can be suppressed by combustion [9–11].
The dynamics of the interaction between a PVC and a swirl flame was recently studied using high-speed imaging measurements in a gas turbine model combustor for partially premixed flames [12,13]. These studies demonstrated that the PVC has a strong influence on flame stabilization, local heat release rate, localized flame extinction, and mixing. This resulted in a complex interaction between the PVC and thermo-acoustic oscillations. Generally, from the knowledge about swirling flames, it can be concluded that the presence or absence of a PVC in a GT-like flame changes the flame shape and dynamics significantly.
A different gas turbine model combustor for lean premixed swirl flames was developed by Turbomeca S.A. and has been investigated in detail [14]. For a specific operating condition, numerical simulations predicted a PVC in the non-reacting flow that was not present under reacting conditions [15]. Measurements, however, indicated that the PVC was still present with the flame [16]. In the study presented here, the same combustor was investigated under different operating conditions than before, under both reacting and non-reacting conditions. High-speed stereoscopic PIV was used to measure the flow fields in both reacting and non-reacting cases and high-speed chemiluminescence of the OH radical was used to measure the heat release in the reacting case.

2 Experiment and Diagnostics

2.1 Burner

A schematic overview of the experimental setup and a cross-section of the burner are provided in Figure 1. The burner is based on an industrial design by Turbomeca S.A. and has been studied before both experimentally [14, 16, 17] and numerically [15, 18]. Dry air at room temperature is fed via a plenum into 12 radial swirler vanes. Fuel is injected directly at high momentum into the swirler vanes through 12 holes (1 mm in diameter). This leads to relatively good mixing ('technical premixing') of the fuel and air before they enter the combustion chamber. The inner surface of the nozzle is formed by a conically shaped center body. The combustion chamber

Correspondence to: christoph.arndt@dlr.de

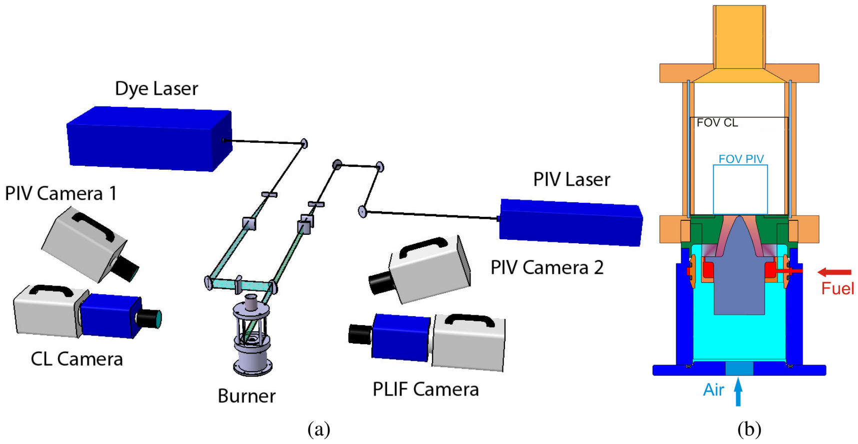

Figure 1: a) Experimental setup b) schematic of the burner with the fields of view for the different measurement techniques.

has a square cross section and consists of four quartz glass plates held in place by a steel post in each corner, thus providing very good optical access. A steel top plate with an exhaust tube in the center forms the exit.
For the reacting case, the burner was operated with a CH_4/air flame at atmospheric pressure (731 g/min air, 35.9 g/min CH_4, $\phi = 0.82$). For the cold-flow studies the fuel was replaced by a nitrogen surrogate at the same volumetric flow rate. Pressure fluctuations in the plenum and in the combustion chamber were measured with two microphone probes (Brüel & Kjær Type 4939).

2.2 Chemiluminescence and Planar Laser-Induced Fluorescence (PLIF)

The chemiluminescence signal of electronically excited OH (termed OH*) in the combustion chamber was imaged at a sustained repetition rate of 5 kHz with a high-speed CMOS-camera (LaVision HSS 5) that was equipped with a two-stage lens-coupled intensifier (LaVision HS-IRO) and a fast f/1.8 UV lens (Cerco). The OH* chemiluminescence signal was isolated by using a high transmission band-pass filter, centered around 310 nm (Laser Components GmbH). OH* was used as a qualitative marker of the heat release of the flame [19]. Simultaneous with the OH* chemiluminescence, PLIF of OH was acquired at a sustained repetition rate of 5 kHz. However, the PLIF measurements will be analyzed in a future study and will not be described here.

2.3 Particle Image Velocimetry (PIV)

The PIV system is based on a diode-pumped solid state (DPSS) dual-cavity laser (Edgewave IS6II-DE), operating at 532 nm and delivering pulse pairs of approximately 2.6 mJ per pulse with an inter-pulse separation of 6 µs repeating at 5 kHz. The laser beam was formed into an approximately 45 mm tall sheet with an approximately 1 mm beam waist in the test section using a three-component cylindrical telescope. Laser light scattering from titanium dioxide particles ($\sim$ 1 µm diameter) was imaged with a pair of high-speed CMOS-Cameras (LaVision HSS 6 and HSS 8) in a stereo-configuration. Velocity vectors were computed via cross-correlation of the image pairs using an adaptive multipass algorithm implemented in a commercial software package (LaVision DaVis 7.2). The final interrogation box size was 16 x 16 pixels with a 50% overlap, resulting in a vector spacing of 0.5 mm and a vector resolution of 1 mm. Laser light reflections off the nozzle caused a large number of spurious vectors to be computed in an isolated region at the nozzle exit. The velocity data in this region was therefore excluded from the subsequent analysis in post-processing.

3 Results and Discussions

The average flow fields for the two examined cases are shown in Figure 2a and 2b. Both flows exhibit the typical features of an enclosed swirl flow, namely an inner (IRZ) and an outer recirculation zone (ORZ) separated by a conical region of high inflow-velocity. However, several differences are immediately recognizable between the two cases. The inflow of the non-reacting case (Figure 2a) has a narrower opening angle, a lower peak velocity,

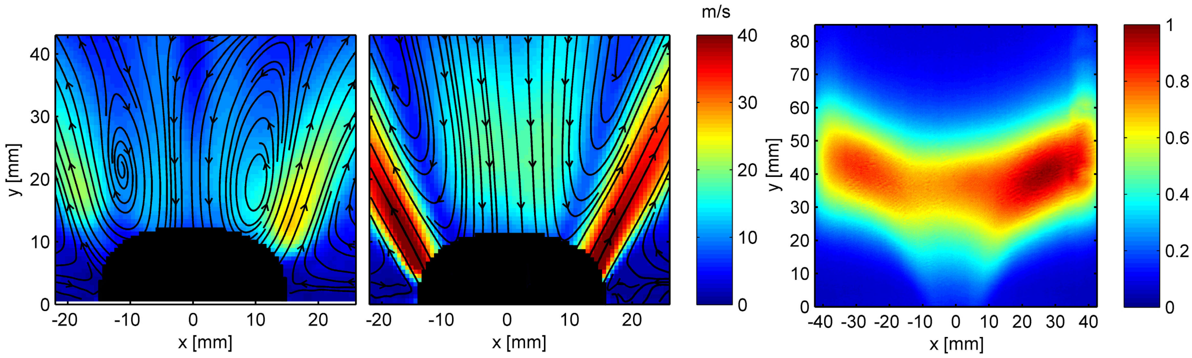

(a) Non-Reacting Mean Flow Field (b) Reacting Mean Flow Field (c) Reacting Mean OH* CL Signal

Figure 2: Average flow fields of a) the non-reacting and b) the reacting case. Color coded is the velocity magnitude and overlayed are the flow contours. The black region indicates the region in which laser reflections caused a large number of spurious vectors to be computed. c) average OH* chemiluminescence. Color coded is the normalized signal intensity.

and penetrates less deeply into the combustion chamber at high velocity than the inflow of the reacting case (Figure 2b). The peak mean velocity magnitude in the the non-reacting case is approximately 27 ms^{-1}, while that of the reacting case is approximately 44 ms^{-1}. This is mainly due to the higher temperature and thus lower density in the reacting flow. In the non-reacting flow, the center of the IRZ is located close to the nozzle, at a height of approximately 20 mm, while the center of the IRZ for the reacting flow is out of the PIV field of view and thus located higher than 45 mm. In Figure 2c, the average OH* chemiluminescence signal is shown. The flame had a conical shape, with the main heat release zone at an axial location between approximately 25 mm and 55 mm above the nozzle. The flame brush extends to $y \approx 65$ mm above the burner exit plate and reaches all the way down into the nozzle. Note that the slight differences in signal intensity on the right and left sides of the image result from a slight asymmetry that is intrinsic to the inflow of the burner. This is also the reason for the left-to-right asymmetry that can be seen in the flow fields.
The frequency spectra of the acoustic signals from the combustion chamber and from the plenum for the two different flows are shown in Figure 3. For the non-reacting case, the pressure signal of the plenum shows no

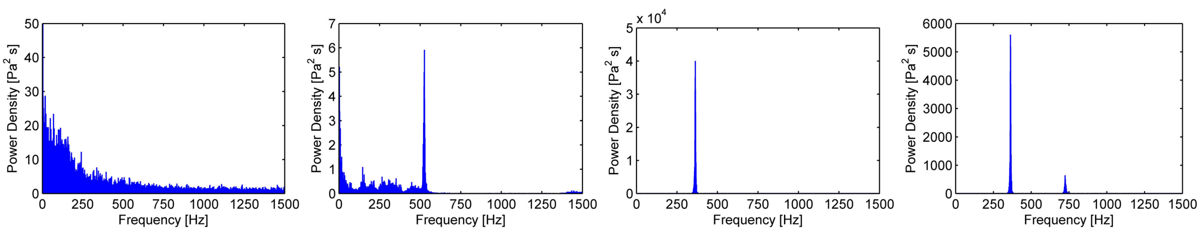

(a) Non-Reacting Plenum (b) Non-Reacting Comb. Chamber (c) Reacting Plenum (d) Reacting Comb. Chamber

Figure 3: Frequency spectra of the acoustic signals from the plenum and from the combustion chamber for a),b) the non-reacting case c),d) the reacting case.

dominant frequencies, while the combustion chamber signal features a dominant mode at 529 Hz. This mode was associated with a precessing vortex core (PVC) structure, as will be shown later. The existence of a PVC in the non-reacting case was predicted by large eddy simulation (LES) [15] and has been observed in the reacting flow [16], albeit under different flow conditions than presented here. For the reacting case, an acoustic pulsation can be seen in both the combustion chamber and the plenum at a frequency of $f \approx 365$ Hz. The second harmonic of this mode, at $f \approx 730$ Hz, also can be seen in the combustion chamber. However, the sound pressure level is relatively low in comparison to other flames studied in this burner [14, 16, 17]. Note that the sound pressure level of the acoustic pulsation is several orders of magnitude larger than the acoustic signal from the PVC.

It has been shown in previous studies that the dominant acoustic frequency is caused by a feedback loop that can be described by an oscillating fuel supply in combination with a convective time delay [14].

To get a deeper insight into the nature of the dominant flow structures, a proper orthogonal decomposition (POD) [20, 21] analysis on a temporal sequence of the vector fields was performed, yielding the eigenmodes of the flow structures, their temporal coefficients, and their contribution to the turbulent kinetic energy. This mathematical tool facilitates the identification of the dominant flow structures and the frequencies of periodic motions. Figure 4 shows the first three POD modes for the non-reacting (top row) and the reacting flows (bottom row), as well as the profiles of the corresponding temporal coefficients. The flow is visualized by the out-of-plane vorticity. In the non-reacting case, mode 1, which represents the average flow field, shows large scale vortical structures in

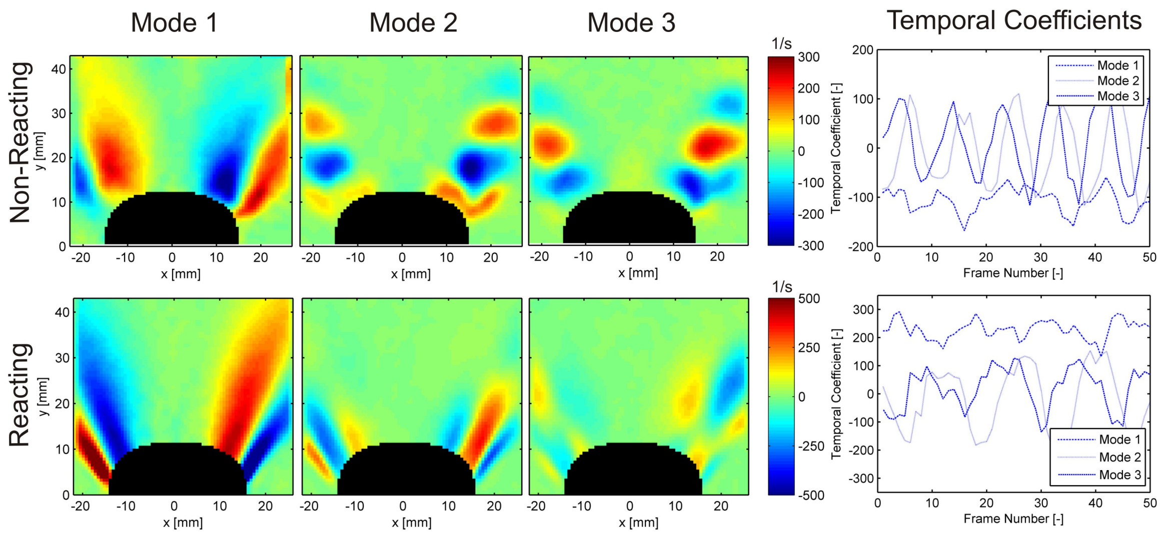

Figure 4: Vorticity fields of POD modes 1-3 for the non-reacting (top row) and the reacting (bottom row) flow and a typical temporal sample of the corresponding temporal coefficients. Color coded is the vorticity in s^{-1}.

the region of the inner (ISL) and outer shear layers (OSL) between the inflow and the recirculation zones. The vorticity fields of mode 2 and 3 show a series of symmetric vortex pairs roughly in the position of the inflow. The power spectra of the temporal coefficients of mode 2 and 3 (not shown) show a dominant frequency of 529 Hz, which also was detected by the microphone in the combustion chamber. The profile of the temporal coefficients of modes 2 and 3 are very similar in shape, with mode 3 leading mode 2 by approximately 90 °. The similarity in shape and dominant frequency of the temporal coefficients of these modes, as well as the similarity in the spatial structure, suggest that they represent the same coherent flow structure, which seems to resemble a PVC. This vortex structure also can be directly identified in the instantaneous PIV vector fields. The frequency of the PVC increases almost linearly with the volumetric inflow.

Mode 1 of the reacting case again represents the mean flow field and shows two elongated vortical structures in the ISL and OSL. Modes 2 and 3 show small scale vortex structures in the region of the ISL and OSL, most probably caused by a fluctuation of the position of the shear layers throughout the acoustic cycle, as will be discussed below. The dominant frequency of the temporal coefficients of the first 3 POD modes and the acoustic signal are the same, namely 365 Hz. The larger vortical structures at $y \geq 20$ mm in mode 3 seem to be the result of a periodic vortex shedding at this frequency. No evidence of a PVC is visible here. As predicted by LES, the PVC seems to be supressed by the combustion.

The dynamic behavior of the PVC-like structure in the non-reacting flow is shown in Figure 5. Here, a phase-correlated averaging of the flow field was performed to identify the PVC motion around the combustor [13]. The velocity field measurements were phase-sorted (with respect to the temporal coefficient of mode 2 of the POD)

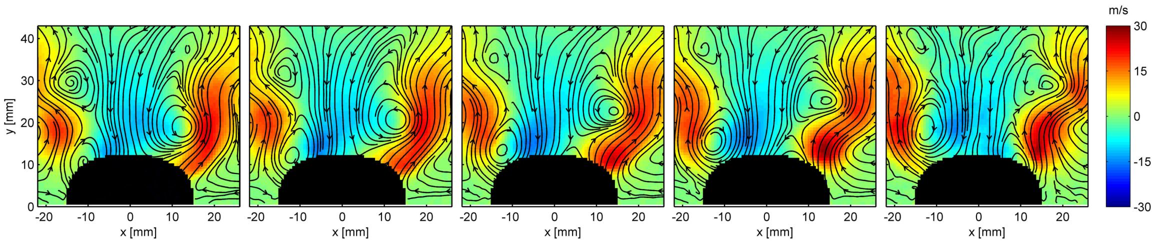

(a) 30 ° (b) 70 ° (c) 110 ° (d) 150 ° (e) 190 °

Figure 5: Phase-averaged sequence of the PVC dynamics in the non-reacting flow. Color coded is the axial velocity component in ms^{-1} and overlayed are the flow contours.

into 18 bins of 20 ° width. Color coded in the image series is the axial velocity component and overlayed are the flow contours. A periodic vortex structure is visible in the region of the shear layer between the inflow and the IRZ. This vortex structure represents a slice through the PVC that was identified in the POD analysis. One can see the vortices forming at the base of the combustion chamber and then propagating upstream. The inflow gets wrapped around those vortices.

Figure 6 shows an acoustically phase-averaged sequence of the flow field dynamics for the reacting case. The procedure for the phase averaging was similar to that for the non-reacting case, with the phase angle being determined from the acoustic measurements. One can see a change in the magnitude of the inflow and backflow velocities in the IRZ throughout the image sequence. The opening angle of the inflow as well as its shape change throughout the acoustic cycle. This radial movement of the inflow explains the small-scale vortical structures in modes 2 and 3 of the POD analysis that were associated with a fluctuation of the shear layer positions. An upwardly convecting symmetric vortex structure is apparent between the inflow and the IRZ. These vortices are associated with a periodic vortex shedding, as was discussed in the POD analysis. The vortices seem to interact with the inflow, i.e. the vortices drag the inflow inwards, and are thus again the reason for the radial motion of the inflow.

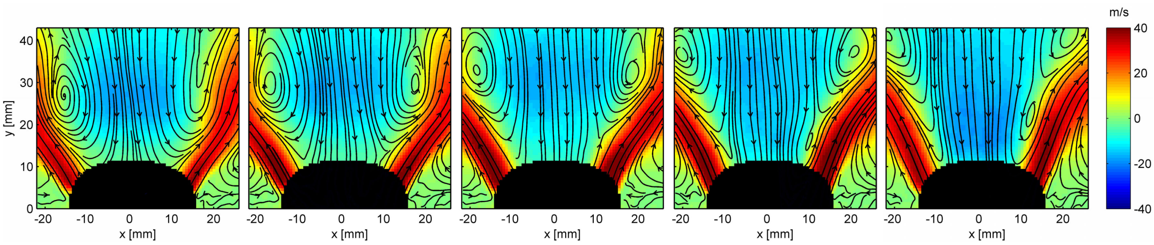

(a) 10 ° (b) 50 ° (c) 90 ° (d) 130 ° (e) 170 °

Figure 6: Phase-averaged sequence of the flow field dynamics in the reacting flow. Color coded is the axial velocity component in ms^{-1} and overlayed are the flow contours.

4 Conclusions

Simultaneous OH* chemiluminescence and stereoscopic PIV measurements have been performed at a sustained repetition rate of 5 kHz in a technically premixed gas turbine model combustor. A confined swirling CH_4 / air flame, and a corresponding non-reacting flow were analyzed. The non-reacting flow contained a precessing vortex core structure, which was identified using both proper orthogonal decomposition and phase averaged flow field analysis. The flow field of the reacting case featured periodic vortex shedding in the inner shear layer that interacted with the inflow. The PVC was damped out in the reacting case, as predicted by LES [15].

References

[1] Gupta AK, Lilley DG, Syred N. (1984). Swirl Flows. Abacus Press.

[2] Lucca-Negro O, Doherty TO. (2001). Vortex Breakdown: A Review. Proc. Energy Combust. Sci. 27: 431.

[3] Syred N. (2006). A review of oscillation mechanisms and the role of the precessing vortex core (PVC) in swirl combustion systems. Prog. Energy Combust. Sci. 32: 93.

[4] Fernandes EC, Heitor MV, Shtork SI. (2006). An analysis of unsteady highly turbulent swirling flow in a model vortex combustor. Exp. Fluids 40: 177.

[5] Spencer A, McGuirk JJ, Midgley K. (2008). Vortex Breakdown in Swirling Fuel Injector Flows. J. Eng. Gas Turbines Power 130: 021503.

[6] Valera-Medina A, Syred N, Griffiths A. (2009). Visualisation of isothermal large coherent structures in a swirl burner. Combust. Flame 159: 1723.

[7] Stöhr M, Sadanandan R, Meier W. (2009). Experimental study of unsteady flame structures of an oscillating swirl flame in a gas turbine model combustor. Proc. Combust. Inst. 32: 2925.

[8] Li G, Gutmark EJ. (2006). Boundary Condition Effects on Nonreacting and Reacting Flows in a Multiswirl Combustor. AIAA J. 44: 444.

[9] Schneider C, Dreizler A, Janicka J. (2005). Fluid Dynamical Analysis of Atmospheric Reacting and Isothermal Swirling Flows. Flow, Turbulence, Combust. 74: 103.

[10] Schildmacher K-U, Koch R, Bauer H-J. (2006). Experimental Characterization of Premixed Flame Instabilities of a Model Gas Turbine Burner. Flow, Turbulence, Combust. 76: 177.

[11] Duwig C, Fuchs, L. (2007). Large eddy simulation of vortex breakdown/flame interaction. Phys. Fluids 19: 075103.

[12] Boxx I, Stöhr M, Carter CD, Meier W. (2010). Temporally resolved planar measurements of transient phenomena in a partially pre-mixed swirl flame in a gas turbine model combustor. Combust. Flame 157: 1510.

[13] Steinberg AM, Boxx I, Stöhr M, Carter CD, Meier W. (2010). Flowflame interactions causing acoustically coupled heat release fluctuations in a thermo-acoustically unstable gas turbine model combustor. Combust. Flame 157: 2250.

[14] Meier W, Weigand P, Duan XR, Giezendanner-Thoben R. (2007). Detailed characterization of the dynamics of thermoacoustic pulsations in a lean premixed swirl flame. Combust. Flame 150: 2.

[15] Roux S, Lartigue G, Poinsot T, Meier U, Bérat C. (2005). Studies of mean and unsteady flow in a swirled combustor using experiments, acoustic analysis, and large eddy simulations. Combust. Flame 141: 40.

[16] Boxx I, Arndt CM, Carter CD, Meier W. (2010). Highspeed Laser Diagnostics for the Study of Flame Dynamics in a Lean Premixed Gas Turbine Model Combustor. Exp. Fluids (online, DOI: 10.1007/s00348-010-1022-x).

[17] Arndt CM, Steinberg AM, Boxx IG, Meier W, Carter CD, Aigner M. (2010). Flow-Field and Flame Dynammics of a Gas Turbine Model Combustor During Transition Between Thermo-Acoustically Stable und Unstable States. Proc. ASME Turbo Expo 2010: GT2010-22830.

[18] Galpin J, Naudin A, Vervisch L, Angelberger C, Colin O, Domingo P. (2008). Large-eddy simulation of a fuel-lean premixed turbulent swirl-burner. Combust. Flame 155: 247.

[19] Docquier N, Candel S. Combustion control and sensors: a review. (2002). Prog. Energy Combust. Sci. 28: 107.

[20] Jolliffe, IT. (2002). Principal Component Analysis. Springer.

[21] Berkooz G, Holmes P, Lumley JL. (1993). The Proper Orthogonal Decomposition in the Analysis of Turbulent Flows. Annu. Rev. Fluid Mech. 25: 539.